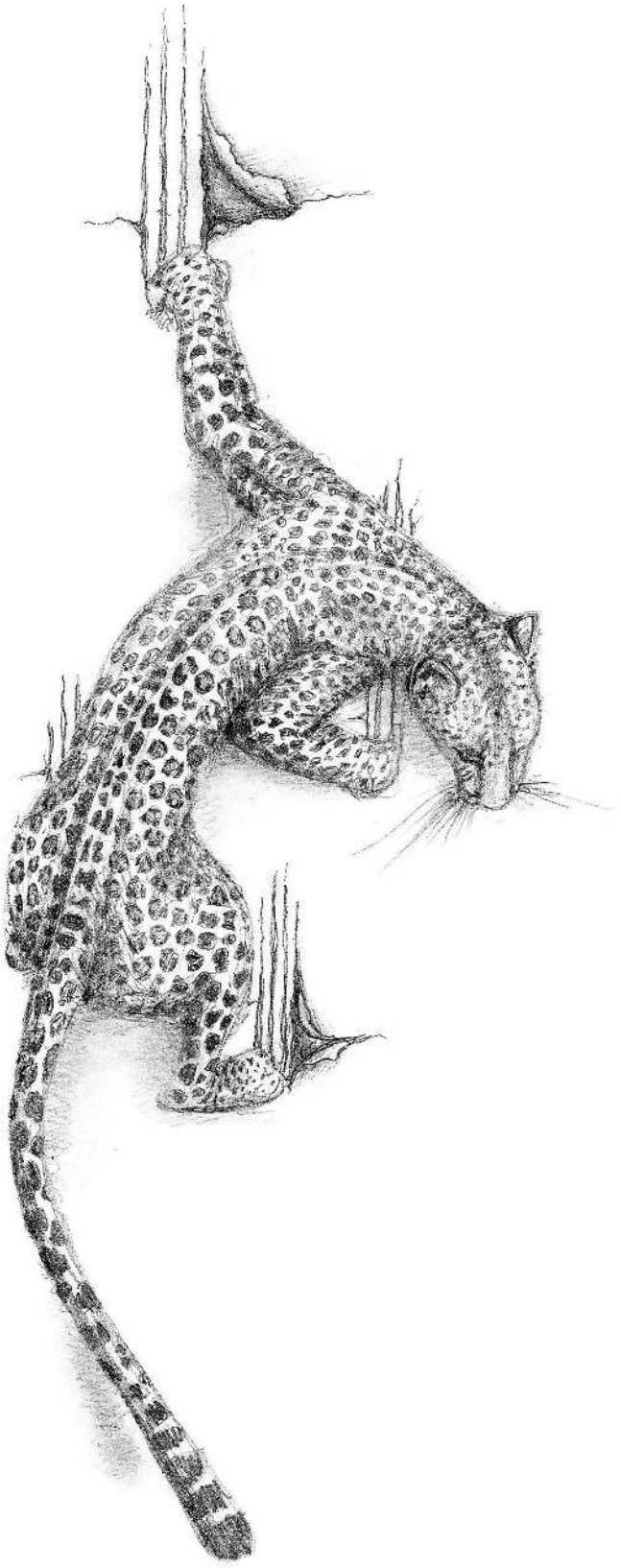

4

Estimating leopard population density in relation to terrain ruggedness with spatially explicit capture-recapture models

4.1 Abstract

The best known international system of classifying species at high risk of global extinction is the IUCN (International Union for Conservation of Nature) Red List, which aims to provide an explicit and objective framework to define species conservation status, and which is based on criteria heavily dependent on population size. In the animal kingdom, large carnivorous mammals are of great scientific and conservation interest; however, demographic information is often scarce. In South Africa, leopard *Panthera pardus* demographic data are sparse and usually collected within protected areas; nonetheless, the leopard population is generally thought to be in decline. Most of the Western Cape studies focused on the Cederberg Mountains and few of them investigated topics dealing with habitat preferences and population density. In this study, camera trap systems were used to collect capture-recapture data and to estimate leopard population density in the Little Karoo, using Spatially Explicit Capture-Recapture (SECR) models. Model selection showed that leopard density varied with topographic relief; it increased with ruggedness of the terrain up to an optimum, and followed a reversed trend as the terrain roughness kept increasing. The parameter estimates of the best-

performing model's detection function showed that the leopard population in the Little Karoo was composed of two groups of individuals with significantly different home range sizes, potentially explained by gender duality in movement. The study estimated the leopard population density to be low; density estimates ranged from 0.49 to 0.82 individual per 100 km^2.

4.2 Introduction

The conservation movement is believed to have started in 1662 when John Evelyn – an English writer, gardener and diarist – submitted a book highlighting the importance of conserving forests to the Royal Society [100]. Due to a number of social and economic factors, the conservation movement only started to gather momentum much later during the 19^{th} century, with the goal to preserve and promote the sustainable use of natural resources [111]. In 1978, an eclectic group of scientists congregated, at what is now called the First International Conference on Conservation Biology, to join forces and save species that were of conservation concern [117]. This event led to a landmark publication in 1980, *Conservation biology: an evolutionary-ecological perspective* [318], and resulted in the creation of a new discipline: conservation biology [347]. One of the most urgent challenges was to develop methods to quantify risk of extinction in order to evaluate whether a species should be listed as endangered. Today, the best known international systems of classifying species at risk of global extinction is the IUCN (International Union for Conservation of Nature) Red List, which aims to provide an explicit and objective framework to define conservation status of species, and which is based on criteria heavily dependent on population size [152].

In the animal kingdom, large carnivorous mammals are of great scientific and conservation interest; however, demographic information is scarce due to challenges rising when conducting research studies on elusive, wide-ranging and low density species [16]. Direct observations and species counts of large carnivores are logistically testing, expensive and time-consuming; several alternative sampling techniques have therefore been developed to estimate their population abundance/density [300, 364]. The most common substitute was to rely on track counts [23, 136, 311], although the methodology remained controversial [20, 66, 322]. Capture-recapture sampling using camera trap data is a method that was first developed to monitor tiger *Panthera tigris* populations in India [163], and is now used extensively worldwide to estimate population density of other individually identifiable species [33, 138, 154, 306, 314, 316, 340].

In southern Africa, leopards are commonly found to be the apex predator outside protected areas, due to their ability to adapt and persist in fragmented habitats and areas that undergo anthropogenic land-use changes [274, 328]. Apex predators are of great ecological importance because they profoundly influence ecosystem structure [69, 286, 335]; however, they commonly are vulnerable and of great conservation concern [14, 274, 335].

In South Africa, leopard demographic data are sparse and usually collected within protected areas [17]; nonetheless, the leopard population is generally thought to be in decline [140, 329]. Scientists focused their leopard research work in the northern parts of the country [17]; the Western Cape Province received relatively little attention [210–213, 248–251, 273, 324, 325]. Most of the Western Cape studies focused on the Cederberg Mountains [210–213, 249] and suffered from small sample sizes and technological limitations [249]. Few of them investigated topics dealing with habitat preferences and population density, although there is an urgent need to provide and monitor baseline estimates of leopard population densities outside protected areas [17].

In this study, camera trap systems were used to collect capture-recapture data and to estimate leopard population density in the Little Karoo, using Spatially Explicit Capture-Recapture (SECR) models [90]. The study considered the impact of specific covariates on density, several submodels were fitted and compared using the Akaike Information Criterion (AIC), an estimator of the relative quality of the collection of statistical models given the data [51, 164, 353]. Submodels were ranked and averaged using Akaike weights. Finally, using the best submodel of the collection, the estimated detection function as well as the relationship between density and selected covariates were quantified and plotted.

4.3 Material and methods

4.3.1 Study area

The Little Karoo is a semi-arid desert located at the southern tip of the African continent [Appendix 1A], within the Cape Fold Belt. It is also described as a mega-ecotone, where the succulent Karoo and the Cape Floristic Provinces intermingle [Introduction, Chapter 1 section 1.3.1].

4.3.2 Data collection

Camera trap data were collected between March 2014 and August 2015 within a study area of 4,327 km^2 (minimum convex polygon). Digital automated cameras (Cuddeback Attack and Ambush, Cuddeback Inc., Green Bay, Wisconsin, USA) were deployed in units called camera trap stations. Each unit consisted of two camera traps facing one another (slightly off-set to avoid simultaneous flash triggers), positioned at an average height of 40 cm, and at a 90° angle with a linear channel such as gravel roads, animal paths and riverlines, along which large felids are habitually known to move [9, 16, 162, 313]. All camera traps were set to take photos with a one-second delay between consecutive triggers, and with an incandescent flash at night.

The camera trap study was undertaken as a series of six (A, B, C, D, E and F) regional surveys (spatially and temporally separated, Table 4.1, Fig. 4.1). Each survey is referred to as a session.

Temporal constraints: SECR models assume population closure, an assumption which can be troublesome and easily violated [124,313]. The trend is to restrict the length of the survey period in order to reduce the risks of assumption violation [163, 306]. The leopard's life span (*c.* 10–15 years) is similar to that of other large felids, such as tiger and jaguar *Panthera onca* [146, 326], which is why the use of a short sampling period of three months made the closure assumption tenable [293,366]. Each sampling block, or session, ran for *c.* three months and camera trap stations were checked once (*c.* 1.5 months, halfway through the survey) to change batteries.

Spatial constraints: Defining the size of the study area and selecting a spatial sampling design were partly driven by a) SECR model assumptions, b) bibliographic knowledge about the home range size of leopards, and c) field-collected information. SECR models assume that all individuals of the targeted population can be detected (i.e. all leopards inhabiting the study area have a probability greater than zero to be photo-captured) [163, 252]. Leopards are well studied in Africa [274] including the northern parts of South Africa [17], and leopard home ranges vary substantially with the productivity of the area in which they occur [11, 35, 189, 233, 320]. Relatively few leopard studies were conducted in the Western Cape, but research in the Cederberg Mountains provided home range estimates spanning from 74 to several hundred square kilometers [210].

Survey A was the first survey of the study. It followed a deloyment design using a regular grid that was positioned to maximise the number of camera stations falling onto riverlines [Introduction]. Random locations provided

few to no data at all, and camera trap stations located along river beds were not nearly as successful as that on roads, both in terms of capture frequency and capture diversity. Because of the high number of camera trap stations along river, the region's unpredictable flash floods threatened the study to suffer from recurrent equipment and data losses. The spatial deployment of camera traps was adjusted throughout survey A and the newly developed design was then consistently applied across survey B, C, D, E and F: camera trap stations were deployed on roads and animal paths to maximise chances of photo-capturing medium to large-bodied animals, with a density of two camera trap stations per 50 km^2. This was achieved using QGIS 2.10.1 software [268] in order to design and place, for each session, a 7×7 km grid across the associated portion of the study area, and to select the two final camera trap sites in each grid cell. The design ensured relatively even sampling effort, to satisfy data collection protocols used to estimate population density using SECR models [16, 56, 57, 110]
The first and last surveys (survey A and F) spatially overlapped; survey F consisted of a replicate of survey A, using the newly chosen and standardised protocol.

Data entry was facilitated by the software Camera Base [338]. The final database was exported into Excel and analysed in R Studio, using the R software 3.2.4 [269].

4.3.3 Density Analysis

Population density estimates were provided by SECR models: a statistical method of estimating population density, which is appropriate for data collected with an array of 'detectors' (camera trap stations) [90].

4.3.3.1 SECR background

Capture-recapture studies are commonly used in ecology to estimate animal population size. Conventional capture-recapture models provide species abundance estimates without incorporating any spatial component in inference. To estimate density, an estimate of the Effective Trapping Area (ETA) is required, which is achieved using ad hoc methods subjected to problematic edge effects [29,89,110,256]. The necessity for a spatial component arose from the observation that animal capture probabilities depend on differential utilisation of space [29]. The SECR approach incorporates spatial information on the location of capture into the capture histories and estimates population density directly without needing to estimate an ETA (i.e. density is an explicit parameter appearing in the likelihood function [90]).

4.3.3.2 SECR inference

SECR models can either be implemented into a maximum-likelihood or Bayesian framework [29]; the former method, which allows the use of likelihood-based methods of model selection, was chosen for this analysis [31, 96]. The likelihood can be defined as the joint distribution of the individuals photo-captured and their capture histories [31,87]. The spatially-explicit maximum likelihood-based approach combines a state model (abundance and distribution of animal home ranges within the landscape) and an observation model (also called spatial detection model). The latter describes the decline in detection probability with distance from the detector to the animal home range centre (activity centre). Among the different functional forms that can be specified for the detection function, the commonly used halfnormal function was selected for this study [96]. Because activity centres are not directly observed, distance is treated like a random effect and conventional distance sampling methods are not used [94].

In this study, models were fitted, using the *secr.fit* function from the *secr* R-package version 3.1.0 [94], by maximizing the full likelihood; which involved integrating all random effects out (i.e. integrating the individuals' activity centres over the unknown locations) [96]. Practically, this was computed by summation over grid cells in the area of integration.

The output of a basic model using a halfnormal detection function gives three parameter estimates: density (D) and two that jointly define the model detection function: g0 (the intercept; probability to photo-capture an individual if the sensor was located onto the individual's activity centre) and σ (scale parameter indicating how quickly the halfnormal detection function falls away as the distance to detector increases) [94].

4.3.3.3 Sampling occasions

Although camera trap data are usually collected continuously, standard SECR models divide the dataset into discrete sampling occasions (e.g. 24-hour periods), which leads to the so-called midnight problem [161]: individuals photo-captured only a few minutes either side of the cut-off time would be recorded twice in their capture history. In this study, the length of each sampling occasion was defined as a 24-hour trap night (starting from 12:00 (noon) to 11:59 on the following day). Leopards are mainly active during the dark hours of the 24-hour daily cycle – between dusk and dawn [16, 165, 210, 271] [Chapter 2 Fig. 2.7(t) and Chapter 3 Fig. 3.1(u)] – making the chosen sampling occasion match the active period of the leopard's diel activity rhythm.

Due to camera failures, the detector sampling effort varied between occasions. These variations were recorded within a usage matrix $K \times S$, where K is the number of detectors and S the number of occasions. The usage matrix was then used as an attribute of the detector dataset in SECR models and camera failures were taken into account when estimating the parameters of interest [91, 95].

4.3.3.4 Data required

SECR models require two types of primary data (i) the locations of the detectors, and (ii) the detection histories of known individuals on one or more sampling occasions (each entry records the detector at which a known individual was photo-captured at each sample occasion).

With traditional traps (causing animal detention), individuals cannot possibly be caught at more than one trap (i.e. detector) during a sampling occasion; therefore, the detection histories show a 2D structure: individual × occasion matrix. Camera traps, however, are considered to be 'proximity detectors', which means that it is possible for an individual to be caught at more than one detector during a sampling occasion, prompting the detection history to have a 3D structure.

With camera traps, it is also possible for individuals to be photo-captured at a detector more than once per sampling occasion; the records of the detection history are count data and follow a Poisson distribution [94], these models are called encounter rate models. In this study, the leopards were rarely photo-captured more than once per sampling occasion which discouraged their use. Instead, each record followed a Bernoulli distribution and each 'cell' of the history contained a binary vector coding presence or absence at each detector [94].

In SECR models, the study area is represented by a 'mask', known as the area of integration: a fine net of points across which values are summed and the likelihood is evaluated [31, 92]. The *secr.fit* function in *secr* R-package version 3.1.0 [94] automatically generates a habitat mask by buffering around the detectors. In this study, the automatic mask process was overridden by the use of the *make.mask* function from the *secr* R-package version 3.1.0 [94], which enabled the construction of the habitat mask from a shape file. Using the *addCovariates* function from the same R-package, specific spatial information (e.g. ruggedness) was defined as spatial covariate attributes to the mask [92].

A sequence of preliminary runs was undertaken, using increasing buffer width values to construct the habitat mask of the likelihood integration.

The buffer argument of the *secr.fit* function depends on the scale of animal movement. Making the region too wide should not significantly affect final estimates because activity centres that are distant from the detectors bring minor contribution to the likelihood. Large buffers can however affect the numerical maximisation of the likelihood and lead to slow computation [90]. The smallest buffer value from which the likelihood and estimates were found stable was then used when fitting multiple density submodels.

4.3.3.5 Age and gender

It was not always feasible to reliably age nor to distinguish the sex of photo-captured leopards. Reliably sexing leopards from photographs is possible due to the striking sexual dimorphism of the species [326]. Without a clear view of the external genitalia, it remains feasible to sex leopards by relying on other morphological measurements: cranial morphology, neck circumferences, body length, shoulder height and chest girth [11]. Depending on the photographs and the posture of the leopard, relative dimensions looked unclear and it sometimes became difficult to gauge body size. Balme et al. (2012) showed that while differentiating mature male leopards ($\geq$ 4 year-old) is unambiguous, distinguishing female leopards from young males can create considerable confusion [15]. Due to similar challenges faced in this study, the sexes were analysed together. However, due to expected gender heterogeneity in movement, a different approach (i.e. finite mixture models) was used to account for such heterogeneity [this is dealt with in more detail in Chapter 4 section 4.3.3.7].

4.3.3.6 Leopard identification

Every photo-capture was either defined as a capture-event or as a duplicate [Chapter 1 section 1.3.3], and all duplicates were discarded for this study. Leopard individuals were identified using their fur patterns, which are unique natural markers made of spots and rosettes, comparable to human finger prints. The markers are visible across the body and the inter-individual variation is sufficient to assign identities [4].

4.3.3.7 Covariates

A variety of submodels can be built by allowing the three principal parameters of the model (D, g0 and σ) to vary with known factors and covariates; examples of model arguments are provided in Table 4.2 and comprehensive instructions and descriptions of these models are provided in Efford. et al (2013) [94].

Fifteen submodels were fitted as part of a first exploratory stage. Only one of the three principal parameters was then allowed to vary with known covariates such as *ruggedness* and *session*. Using the first results of the AIC model selection [51,164,353], a set of 12 additional submodels was defined to assess whether more complicated models – assuming more complex biological explanations – would receive more AIC weight. Model computations were performed using facilities provided by the University of Cape Town's ICTS High Performance Computing team (UCT HPC Cluster): http://hpc.uct.ac.za.

ruggedness: spatial covariate
Heterogeneous topographic relief – especially in mountainous regions – often is an essential constituent of the niche of a species [50,246,361]. In the Little Karoo, leopards' strongly avoid even terrain [Chapter 1 section 1.8(u)]; the Terrain Roughness (ruggedness) Index (TRI) [284], calculated using QGIS 2.10.1 software [268], was used as a geospatial covariate of density in SECR models. Using the *addCovariates* function from the *secr* R-package version 3.1.0 [94], spatial covariate TRI was added to the constructed habitat mask.

session: sampling blocks
The study was undertaken as a series of six regional surveys (temporally and spatially separated). In SECR modelling, the six sampling blocks are called 'sessions' and are treated independently, ignoring individual photo-recaptures across sessions [93]. The *secr.fit* function fits a multi-session model by maximising the product of session-specific likelihoods [96], and the default is to treat all parameters (D, g0 and σ) constant across sessions; however, models with session-specific parameters can also be specified. Distinct values of density (D) and detection probabilities (g0) were also fitted, enabling to calculate different estimates for the six sessions.

Modelling sessions independently implied a loss of information because individual photo-recaptures across sessions were ignored. Alternatively, specifying a single session model would have led to problems with the assumption of demographic closure, which is why this option was not explored.

b: behavioural effect
Models in capture-recapture studies of carnivores commonly include a behavioural effect whereby the detection probability changes after initial capture, especially when it involves retention of the species of interest [61, 102, 256]. Camera traps are non-invasive and although it is not expected that they could affect leopard behaviour, several studies using camera traps to estimate population density confirmed a behavioural response among individuals [30, 355, 356]. In Royle et al. (2009) and Borchers et al. (2014), this response was interpreted as a factor related to trail use rather than an actual

behavioural effect [30, 292]. The hypothesis of a learning process within the animals with respects to detectors was tested in this study by fitting formula 'b' on g0 in SECR models [86].

h2: individual heterogeneity
Compared to standard capture-recapture models, SECR models account for some individual heterogeneity due to the incorporation of differential space use among targeted individuals; howver, one of the most tenacious problems in capture-recapture studies remains individual heterogeneity: the variation in detection probability among individuals [88]. Whenever possible, this variation is accounted for by grouping individuals into homogeneous classes, e.g. based on gender (male, female) or age (juvenile, adult). When heterogeneity remains, SECR provides finite mixture models that assume latent individual classes. These models calculate, for each class: 1) different detection parameters and 2) the proportion of individuals in the different latent classes [31,88,264]. In this study, g0 and σ were the two parameters modelled with two-class finite mixture models ($h2$). Three-class ($h3$) finite mixture models were also used to test the hypothesis of having capture probabilities varying with three homogeneous classes: 1) adult male, 2) adult female and 3) juveniles. It was chosen not to present the results because $h3$ models were not yet fully tested. The $h3$ model developer also highlighted the risk of getting stuck on a local maximum of the likelihood during convergence and advised against their use [Efford (2017) personal communication]. Moreover, the standard errors of the parameter estimates were not always estimated or took abnormally high values, suggesting that the models were unstable and did not converge successfully.

4.4 Results

The trapping effort of 17,631 camera trap nights resulted in 26,312 photo-captures of 91 different species. Fifty one (56.04%) species were mammals and 1.34% of all photo-captures were leopards [Appendix 2A].

4.4.1 Descriptive statistics

The study provided 219 photo-captures of leopards, collected at 79 (35%) camera trap stations (Fig. 4.2). Six of these photographs were considered to be dependent events and were discarded; all photographs of the same individual collected within the same trap night following the first photo-capture, at the same location, are considered to be duplicates [Chapter 1 section 1.3.3]. Leopard capture rate was 1.21 in 100 camera trap nights.

Six of the photographs were taken during early mornings, shortly after the automatic deactivation of the incandescent flash, resulting in blurry images and preventing any possible individual identification. These photos were discarded for the purpose of this analysis.

The number of photo-captures collected for each identified individual leopard varied noticeably across the study as a whole (Table 4.3), and across regional surveys (Table 4.4). Among the 219 leopard photo-captures recorded when both cameras of a camera trap station were active, 150 were recorded by both cameras and the remainder by one camera only. It provided a set of 369 photographs (instead of 438 assuming perfect detection). These figures indicate a possible detection failure rate of 15.7% per camera trap, and of 2.4% (0.157^2) per camera trap station.

Based on 207 ($219 - 6 - 6$) photo-captures, twenty nine leopards were identified. Due to detection failures, not all capture events provided simultaneous photos of both flanks of the individuals. This problem was overcome by the collection of photo-recaptures, except for one individual for which only the right flank was recorded. The photo-capture counts and capture histories for the 29 individuals, are respectively provided in Table 4.5 and 4.6.

4.4.2 SECR model selection

The smallest buffer value from which the likelihood and estimates were found to be stable was 10,000 meters; it was therefore defined as such in all submodels of the first and secondary exploratory stages. Models were ranked according to Akaike's Information Criterion, and AIC weights were calculated [51]. In the first exploratory stage, the finite mixture model that used $h2$ as a covariate of parameter σ (Model 2) was the best-performing one (Table 4.7). In the second exploratory stage, the models that used regression splines for density surface modelling, along with $h2$ and session as covariates of parameter σ (Models 21 and 22) were the best-performing ones (Table 4.8). There was little difference between the AIC weights of Models 21 and 22 (0.01), suggesting that they both fitted the data similarly [332].

4.4.3 Detection function

The two best-performing models, Models 21 and 22, produced respectively 12 and 13 β coefficients estimated on the link scale (Appendix 5A.1 and 5A.2); the real parameter values (fitted values) were calculated by back-transforming the β parameters on the scale given by the link function: log-transformation of D and σ, and logit transformation of g0 and pmix (Table 4.9). In this

analysis, the detection function was jointly defined by g0 (detection probability) and σ (index of home range size), and modelled as a halfnormal function. Models 21 and 22 had the same specified detection functions and their shapes were very similar (Fig. 4.3). In each graph, 12 detection functions were represented further to σ varying with two classes of individuals ($\sim h2$) and with six sessions ($\sim session$). Two of the 12 curves were difficult to distinguish because they overlapped with other two (very little difference in σ between session B and F). All curves had the same intercept: g0 (the probability to detect an individual over a 24-hour occasion when the detector is located at its activity centre) which was defined as a constant parameter in both model formulas (Table 4.8) and estimated at 0.029, 95% confidence interval 0.023–0.036 (Table 4.9). Parameter σ varied substantially between the two latent classes of individuals that are quantified by parameter pmix (Table 4.9). In Model 21, with class $h2 = 1$ making 69% of the population, σ ranged from 1412.04 to 1966.38 m; with class $h2 = 2$ making 31% of the population, σ ranged from 4414.09 to 7411.48 m. The estimated σ was 3.13 times ($e^{1.14}$, Table 4.9) greater for class 2 compared to class 1, resulting into different shapes of their respective detection functions: in the case of class 2, the function fell away more gradually with distance (class 2 individuals were more detectable at greater distances). The pmix parameter estimated what proportion of the population fell into these latent classes (Table 4.9). Model 21 estimated 69% (95% confidence interval 51–84%) of the population to be in class 1 and 31% (95% confidence interval 16–49%) to be in the second class that has wider ranging movement. Model 22 produced very similar estimates.

4.4.4 Number of individuals

The expected number of leopards N in each of the six regional surveys (A, B, C, D, E and F), estimated by the *region.N* function from the *secr* R-package version 3.1.0 [94], was close between Models 21 and 22 (Table 4.9). With model 22, it ranged from 9.49 individuals in session C (95% confidence interval 6.36–14.11) to 17.11 in session F (95% confidence interval 11.61–25.19). With the multi-session approach, the estimation of leopard abundance was constrained to each session independently, preventing the estimation of a single abundance number of leopards for the study area as a whole. It was not viable to add up the expected number of leopards from each survey due to habitat mask overlap and the fact that individuals caught across more than one survey would be counted twice. The averaged leopard density estimates $\overline{D}$, computed for each session by dividing the expected number of leopard N by the area of the session's habitat mask, ranged from 0.49 to 0.82 individual

per 100 km^2 with Model 21, and from 0.51 to 0.82 individual per 100 km^2 with Model 22 (Table 4.10).

4.4.5 Density maps

The best-performing models, Models 21 and 22, allowed density to vary with spatial covariate *ruggedness* (Table 4.10). Fig. 4.4 shows, for both models, the relationship between the leopard population density in the Little Karoo and the Terrain Ruggedness Index (*ruggedness*). There was a quadratic effect of *ruggedness* on leopard density. With Model 22, the leopard density was estimated around 0.08 leopards per 100 km^2 in flat terrain, TRI = 10. This density estimate increased with terrain ruggedness (7.73 leopards per 100 km^2 in moderately-rugged terrain, TRI = 50) up to 20.62 leopards per 100 km^2 in optimal terrain, TRI = 89. The trend was then reversed and leopard density was estimated around 17.57 leopards per 100 km^2 in highly-rugged terrain, TRI = 110). Using the constructed habitat masks for the six regional surveys A, B, C, D, E and F (Fig. 4.5), predicted density maps were produced for Model 22 (Fig. 4.6). These maps are chloropleth maps: shaded graphical representations in which each geographical area (habitat mask grid cell) had a *ruggedness* value, and was shaded according to its associated density estimate.

4.5 Discussion

Using remote camera trapping in conjunction with SECR modelling, this chapter estimated leopard density in the Little Karoo. The study enabled us to identify 29 leopard individuals in an arid and inaccessible landscape, highlighting the feasibility of using linear channels such as roads and animal paths to sample wide-ranging, low density species such as leopards in the Little Karoo.

Model selection showed that leopard density varied with topographic relief, which is often an essential constituent of the niche of a species [50,246,361]. Leopard density estimates increased with ruggedness of the terrain up to an optimum (20.6 leopards per 100km^2 in terrain with TRI = 89); it followed a reversed trend as the terrain roughness kept increasing. The two best models were almost identical apart from one extra degree of freedom used in the spline function of Model 22 compared to that of Model 21, which allowed the density-*ruggedness* relationship to fall away more gradually after reaching its optimal peak. These results support the observation developed by Skinner et al. (1990) that leopards of the Western Cape

Province prefer to hunt in rugged and rocky terrain where prey is abundant and where the landscape is more appropriate to stalk, kill [310], and store food items under rocky overhangs. However, this affinity for rugged mountain terrain decreased when TRI exceeded 100, which usually translated into a barren landscape with steep slopes; the decline in leopard density might be explained by a drop of prey presence due to the reduction in vegetation cover, and by difficulties in manoeuvring successful hunts in steep and rugged rockslide areas.

The parameter estimates of the best-performing model's detection function showed that the leopard population in the Little Karoo was composed of two groups of individuals with significantly different σ parameters (3.13 to 1 ratio), which can be used as an index of home range. Using the estimated values of σ and the formula HR $= 2.45^2 \cdot \pi \cdot \sigma^2$ [53], the 95% home range area for the individuals of the two latent classes ranged from $37.88\,\mathrm{km}^2$ to $106.72\,\mathrm{km}^2$ (less mobile group), and from $370.18\,\mathrm{km}^2$ to $1043.53\,\mathrm{km}^2$ (more mobile group) across the six sessions. In the Cederberg Mountains, male leopards were found to range across areas 4.4 times larger than that of females, and female home ranges were entirely incorporated into that of males [213]. Gender differences in movement could also be explained by males moving in a more linear fashion to patrol their territories and keep other competing males away from potential mating females [213], while females were observed to move in an unpredictable and undefined manner while searching for food [184]. This gender duality in home range sizes could also explain the individual heterogeneity observed in the Little Karoo as well as the associated and uneven population ratio (69–31%); slightly more than two third of the leopard population would be females with home ranges incorporated into that of territorial males, the latter making for slightly less than one third of the population. This could however not be tested because it was not always feasible to reliably sex photo-captured leopards.

Model selection showed that g0, the probability to detect an individual over a 24-hour occasion when the detector is located at its activity centre, was constant and did not vary with latent classes ($h2$). This was expected because of the absence of explicit biological explanation to justify individual heterogeneity in detection probability at the activity centre.

The parameter estimates of the best-performing model's detection function also showed that σ (i.e. leopard home range) varied across sessions. Because the series of six sessions was spatially and temporally separated, several factors could have affected leopard movement including seasonality (the view that leopards use the landscape differently in summer and winter is

widely held by farmers [249]), land-use, prey availability/catchability (Balme et al. showed a degree of specialisation in leopard's feeding habitat selection likely to influence local use of the landscape [13]) and other spatial covariates differing from ruggedness.

Differences in ruggedness between the habitat masks of each session could have led to the density parameter estimate (D) varying between sessions. However, *ruggedness* was used in the spatial model for density, and, in the presence of this covariate, the *session* variable did not appear to contain further important information about density, eplaining why *session* was then not selected as a factor affecting density.

Leopard density being defined as a function of ruggedness, it was more appropriate to provide density maps than a single accurate estimate of density for the study area as a whole. However, in order to compare those results to bibliographical leopard density estimates previously calculated within the Western Cape Province, averaged leopard density estimates $\overline{\mathrm{D}}$ were computed. Those estimates, ranging from 0.49 to 0.82 leopard individuals per $100\,\mathrm{km}^2$, were similar but smaller than those provided by Martins (2010) for the leopard population of the Cederberg Mountains (1.1–1.5 individuals per $100\,\mathrm{km}^2$), and by Mann (2014) for the leopard population of the eastern section of the Little Karoo (1.18 individuals per $100\,\mathrm{km}^2$) [208, 213]. Martins (2010) surveyed portions of the Cederberg Mountains where the human population (http://www.statssa.gov.za, 2017) and the degree of human disturbance were smaller than in the Little Karoo [213], which could have contributed to greater leopard densities. The eastern section of the Little Karoo, surveyed by Mann (2014), is more mountainous than our study site and might provide more suitable habitat for leopards.

Carnivore population density is usually closely related to the density of available prey [57]. The landscapes of the Western Cape Province cannot support large herds of herbivores because the nutrient-poor soils on which the vegetation grows do not provide enough nitrogen for the protein requirements of large herds, and prey densities remain low [34,196,270]. This could explain the low density of leopard population in the Little Karoo [212, 213, 251], as well as the small body size of the leopards in the Cape Fold Belt [11, 213].

4.6 Tables

Table 4.1: Camera trap deployment
Given the vastness of the study area in the Little Karoo, the camera trap study was undertaken as a series of six regional surveys: A, B, C, D, E and F. For example, survey C consisted of 34 camera trap stations deployed following a grid-layout, with an average camera spacing of 3265 m. It ran for 102 nights, during which 19 leopard photo-captures were collected and four leopard individuals were identified.

	A	B	C	D	E	F
Camera trap stations	57	38	34	31	30	32
Camera spacing (m)	2122	3330	3265	3253	3817	3531
Occasions	120	103	102	113	95	104
Detections	45	26	19	23	46	48
Individuals	6	5	4	7	10	10

Table 4.2: Model arguments in *secr.fit*
The formula for any detection parameter (g0, D, σ) may be constant (~ 1, the default) or some combination of terms in standard R formula notation. For example, $g0 \sim b+h2$ specifies a model with a learned response and a 2-class finite mixture for heterogeneity.

Parameter predictors	Information
g0, detection probabilities	
~ 1	g0 is constant across animals, occassions and detectors
$\sim session$	session-specific g0
$\sim b$	learned response
$\sim h2$	2-class finite mixture for heterogeneity in g0
D, density	
~ 1	density is contant
$\sim session$	session-specific density
$\sim ruggedness$	ruggedness affects density in a linear manner
$\sim ruggedness + ruggedness^2$	ruggedness affects density in a quadratic manner
$\sim spline(ruggedness, k)$	ruggedness affects density according to a spline regression
sigma, detection function	
~ 1	sigma is constant across animals, occasions and detectors
$\sim h2$	2-class finite mixture for heterogeneity in sigma
$\sim session$	session-specific sigma

Table 4.3: Photo-capture heterogeneity
The total number of photo-captures collected in the Little Karoo for each identified individual leopard varied noticeably, ranging from one to 54. For example, seven individuals were photo-captured once, while four other individuals were photo-captured twice. The most photo-captured individual of all identified leopards was photographed 54 times.

Photo-capture categories	1	2	3	5	7	8	11	12	13	14	20	22	54
Number of individuals	7	4	4	5	1	1	1	1	1	1	1	1	1

Table 4.4: Photo-capture heterogeneity in each survey
The number of identified leopard individuals in the Little Karoo and associated photo-captures varied across surveys. For example, 20 photo-captures collected throughout survey C enabled to identify four leopard individuals. Two of them were photo-captured twice, one was photo-captured three times, whereas the fourth one was photo-captured 13 times.

Survey	Number.of	Cat1	Cat2	Cat3	Cat4	Cat5	Cat6	Tot.capt	Tot.ind
Survey A	captures	1	2	3	7	31		45	
	individuals	2	1	1	1	1			6
Survey B	captures	1	4	9	11			26	
	individuals	2	1	1	1				5
Survey C	captures	2	3	13				20	
	individuals	2	1	1					4
Survey D	captures	1	2	3	5	10		23	
	individuals	3	1	1	1	1			7
Survey E	captures	1	2	3	5	12	13	49	
	individuals	1	2	3	2	1	1		10
Survey F	captures	1	2	3	7	8	23	50	
	individuals	4	1	2	1	1	1		10

Table 4.5: Photo-capture counts

Several leopard individuals of the Little Karoo were photo-captured across several surveys (e.g. LEO 10 was photo-captured nine times throughout survey B and 13 times throughout survey C). NONID accounts for photo-captures that did not allow individual identification.

Individual	A	B	C	D	E	F	Total	Individual	A	B	C	D	E	F	Total
LEO 01	2						2	LEO 16				1	13		14
LEO 02	31					23	54	LEO 17				3	5		8
LEO 03	1						1	LEO 18				2			2
LEO 04	7				12	1	20	LEO 19				1			1
LEO 05	1						1	LEO 20					5		5
LEO 06	3					8	11	LEO 21					3		3
LEO 07		11		1		1	13	LEO 22					1		1
LEO 08		4				1	5	LEO 23					2		2
LEO 09		1					1	LEO 24					2	3	5
LEO 10		9	13				22	LEO 25					3	2	5
LEO 11		1					1	LEO 26					3		3
LEO 12			2	10			12	LEO 27						3	3
LEO 13			2				2	LEO 28						7	7
LEO 14			3				3	LEO 29						1	1
LEO 15				5			5	NONID	1	1		1	2	1	6

Table 4.6: Photo-capture histories

After assigning leopard identities in the Little Karoo, photo-capture histories were built by listing for each photo-capture: 1) the camera trap station (e.g. A43) and 2) the sampling occasion (e.g. 009). The first letter of the camera trap station ID indicates the survey ID (e.g. A43 is a camera trap station deployed during survey A). Leopard LEO 01 was photo-captured twice during survey A, at camera trap station A43 on the 9th camera trap night, as well as at camera trap station A42 on the 72nd camera trap night.

Individual	History						
LEO 01	A43 (009)	A42 (072)					
LEO 02	A04 (005)	A02 (011)	A43 (030)	A04 (035)	A29 (041)	A33 (046)	A29 (052)
	A29 (061)	A33 (065)	A04 (066)	A20 (067)	A43 (069)	A29 (069)	A04 (071)
	A33 (074)	A23 (081)	A24 (084)	A39 (085)	A43 (086)	A29 (093)	A11 (094)
	A24 (095)	A29 (096)	A24 (102)	A23 (102)	A11 (102)	A11 (103)	A23 (106)
	A11 (111)	A11 (114)	A39 (117)	F16 (009)	F22 (017)	F17 (032)	F28 (033)
	F16 (036)	F17 (037)	F16 (042)	F11 (043)	F20 (047)	F17 (053)	F11 (064)
	F04 (064)	F14 (067)	F14 (067)	F26 (072)	F20 (072)	F17 (083)	F16 (090)
	F06 (094)	F17 (095)	F04 (095)	F20 (101)	F16 (101)		
LEO 03	A01 (110)						
LEO 04	A06 (013)	A17 (085)	A39 (086)	A11 (094)	A11 (095)	A39 (96)	A01 (117)
	E04 (020)	E14 (026)	E20 (033)	E20 (033)	E12 (034)	E02 (041)	E07 (041)
	E13 (043)	E07 (060)	E08 (075)	E02 (079)	E11 (082)	F13 (086)	
LEO 05	A05 (097)						
LEO 06	A29 (011)	A29 (051)	A29 (073)	F16 (011)	F17 (022)	F16 (049)	F17 (054)
	F16 (067)	F17 (095)	F17 (095)	F17 (099)			
LEO 07	B03 (024)	B06 (031)	B11 (032)	B03 (033)	B03 (051)	B03 (059)	B05 (061)
	B12 (062)	B03 (075)	B06 (089)	B12 (091)	D05 (075)	F31 (058)	
LEO 08	B03 (006)	B03 (021)	B03 (029)	B01 (078)	F19 (014)		
LEO 09	B06 (087)						
LEO 10	B35 (022)	B36 (023)	B37 (053)	B36 (054)	B37 (089)	B36 (089)	B37 (090)
	B36 (093)	B37 (094)	C26 (002)	C16 (014)	C15 (017)	C15 (017)	C26 (021)
	C15 (030)	C22 (034)	C26 (045)	C18 (051)	C16 (064)	C19 (065)	C19 (086)
	C16 (091)						
LEO 11	B36 (100)						
LEO 12	C08 (021)	C08 (039)	D28 (007)	D29 (019)	D28 (026)	D28 (037)	D31 (041)
	D31 (046)	D28 (079)	D29 (092)	D28 (095)	D31 (097)		
LEO 13	C25 (063)	C25 (087)					
LEO 14	C29 (047)	C19 (076)	C29 (082)				
LEO 15	D31 (007)	D28 (012)	D28 (024)	D28 (025)	D28 (094)		
LEO 16	D19 (028)	E29 (018)	E22 (022)	E27 (028)	E29 (029)	E29 (041)	E29 (041)
	E21 (043)	E25 (043)	E29 (047)	E22 (059)	E29 (063)	E29 (073)	E29 (088)
LEO 17	D14 (008)	D15 (009)	D14 (040)	E15 (021)	E20 (024)	E20 (033)	E20 (063)
	E20 (085)						
LEO 18	D29 (039)	D29 (075)					
LEO 19	D15 (028)						
LEO 20	E27 (009)	E28 (023)	E26 (032)	E30 (068)	E27 (086)		
LEO 21	E29 (004)	E29 (011)	E25 (019)				
LEO 22	E22 (013)						
LEO 23	E30 (039)	E30 (071)					
LEO 24	E02 (046)	E02 (046)	F03 (017)	F02 (066)	F03 (078)		
LEO 25	E04 (020)	E03 (047)	E03 (085)	F13 (028)	F09 (029)		
LEO 26	E12 (009)	E14 (026)	E10 (091)				
LEO 27	F27 (041)	F27 (046)	F27 (095)				
LEO 28	F17 (006)	F16 (029)	F17 (054)	F16 (071)	F21 (084)	F17 (085)	F17 (095)
LEO 29	F09 (070)						
NON ID	A04 (043)	B36 (086)	D20 (007)	E03 (076)	E07 (083)	F20 (084)	

Table 4.7: AIC model selection, phase one

Fifteen models – where only one of the three principal parameters (g0, D, σ) was allowed to vary with covariates, were fitted and then compared using the Akaike Information Criterion (AIC), an estimator of the relative quality of the collection of statistical models given the data [51, 164, 353].

Model	g0 $\sim$	D $\sim$	$\sigma \sim$	ΔAIC	AIC weight
1	1	1	1	31.82	0
2	1	1	*h2*	0.00	1
3	*session*	1	1	27.67	0
4	*b*	1	1	31.20	0
5	*h2*	1	1	16.73	0
6	*b* + *h2*	1	1	16.18	0
7	1	*session*	1	30.07	0
8	1	*ruggedness*	1	29.55	0
9	1	*ruggedness* + $ruggedness^2$	1	29.55	0
10	1	spline(*ruggedness*, k=3)	1	25.03	0
11	1	spline(*ruggedness*, k=4)	1	25.00	0
12	1	*ruggedness* + *session*	1	28.26	0
13	1	*ruggedness* + $ruggedness^2$ + *session*	1	28.26	0
14	1	spline(*ruggedness*, k=3) + *session*	1	25.03	0
15	1	spline(*ruggedness*, k=4) + *session*	1	24.99	0

Table 4.8: AIC model selection, phase two

Twenty-seven models were fitted and then compared using the Akaike Information Criterion (AIC), an estimator of the relative quality of the collection of statistical models given the data [51, 164, 353].

Model	g0 ∼	D ∼	σ ∼	ΔAIC	AIC weight
1	1	1	1	47.21	0.00
2	1	1	*h2*	15.39	0.00
3	*session*	1	1	43.05	0.00
4	*b*	1	1	46.59	0.00
5	*h2*	1	1	32.12	0.00
6	*b* + *h2*	1	1	31.57	0.00
7	1	*session*	1	45.45	0.00
8	1	*ruggedness*	1	44.94	0.00
9	1	*ruggedness* + $ruggedness^2$	1	44.94	0.00
10	1	spline(*ruggedness*, k=3)	1	40.41	0.00
11	1	spline(*ruggedness*, k=4)	1	40.39	0.00
12	1	*ruggedness* + *session*	1	43.65	0.00
13	1	*ruggedness* + $ruggedness^2$ + *session*	1	43.65	0.00
14	1	spline(*ruggedness*, k=3) + *session*	1	40.41	0.00
15	1	spline(*ruggedness*, k=4) + *session*	1	40.38	0.00
16	1	1	*h2* + *session*	9.00	0.00
17	1	1	*h2* * *session*	4.57	0.04
18	1	*session*	*h2* + *session*	6.28	0.02
19	1	*ruggedness*	*h2* + *session*	5.77	0.02
20	1	*ruggedness* + $ruggedness^2$	*h2* + *session*	5.77	0.02
21	1	spline(*ruggedness*, k=3)	*h2* + *session*	0.08	0.42
22	1	spline(*ruggedness*, k=4)	*h2* + *session*	0.00	0.43
23	1	*session*	*h2*	13.47	0.00
24	1	*ruggedness*	*h2*	11.91	0.00
25	1	*ruggedness* + $ruggedness^2$	*h2*	11.91	0.00
26	1	spline(*ruggedness*, k=3)	*h2*	6.67	0.02
27	1	spline(*ruggedness*, k=4)	*h2*	6.61	0.02

Table 4.9: Parameter estimates

The table provides, for Model 21 (left) and 22 (right), the real parameter estimates (fitted value) for g0, σ and the mixing proportion pmix of the two classes defined by $h2$. It also gives estimates of the expected number N of leopard individuals occurring in each session taking place in the Little Karoo.

	Estimate	SE	LCL	UCL	Estimate	SE	LCL	UCL
g0	0.029	0.003	0.023	0.036	0.029	0.003	0.023	0.036
σ, session A, $h2 = 1$	1412.042	212.918	1052.490	1894.423	1413.060	213.700	1052.300	1897.400
σ, session A, $h2 = 2$	4414.093	378.506	3732.373	5220.328	4408.654	376.734	3729.927	5210.888
σ, session B, $h2 = 1$	1869.391	316.400	1344.770	2598.678	1875.100	316.615	1349.976	2604.674
σ, session B, $h2 = 2$	5843.785	613.525	4759.632	7174.887	5850.349	613.203	4766.598	7180.550
σ, session C, $h2 = 1$	2370.888	407.251	1697.307	3311.780	2376.426	409.934	1698.897	3324.157
σ, session C, $h2 = 2$	7411.480	970.639	5739.864	9569.919	7414.259	964.712	5751.452	9557.802
σ, session D, $h2 = 1$	1559.817	276.636	1104.789	2202.258	1572.580	278.900	1138.330	2220.293
σ, session D, $h2 = 2$	4876.045	807.224	3532.675	6730.259	4906.352	801.702	3569.331	6744.202
σ, session E, $h2 = 1$	1966.382	344.681	1398.269	2765.318	1969.800	347.937	1397.287	2777.089
σ, session E, $h2 = 2$	6146.980	574.513	5120.108	7379.798	6145.840	581.544	5107.596	7395.133
σ, session F, $h2 = 1$	1865.298	232.937	1461.711	2380.310	1863.453	233.525	1459.025	2379.985
σ, session F, $h2 = 2$	5830.987	542.622	4860.730	6994.920	5813.826	539.125	4849.508	6969.897
pmix	0.696	0.086	0.507	0.836	0.694	0.085	0.508	0.834
N, session A	15.256	2.971	10.453	22.266	15.425	3.012	10.558	22.535
N, session B	10.342	2.261	6.772	15.794	10.022	2.172	6.586	15.251
N, session C	9.649	1.936	6.537	14.244	9.486	1.943	6.375	14.113
N, session D	10.691	2.345	6.991	16.350	10.435	2.190	6.947	15.675
N, session E	14.615	2.983	9.837	21.715	14.489	2.901	9.824	21.370
N, session F	16.710	3.533	11.091	25.174	17.105	3.412	11.614	25.192

Table 4.10: Averaged density estimates $\overline{D}$

The table provides, for Model 21 (left) and 22 (right), the expected number N of leopard individuals occurring in each session of the Little Karoo, as well as the resulting averaged leopard density estimate, $\overline{D}$, given in number of individuals per 100 km^2.

	Mask Area (km^2)	N	$\overline{D}$	N	$\overline{D}$
session A	1870	15.26	0.82	15.42	0.82
session B	2036	10.34	0.51	10.02	0.49
session C	1860	9.65	0.52	9.49	0.51
session D	1880	10.69	0.57	10.44	0.56
session E	2190	14.62	0.67	14.49	0.66
session F	2076	16.71	0.81	17.11	0.82

4.7 Figures

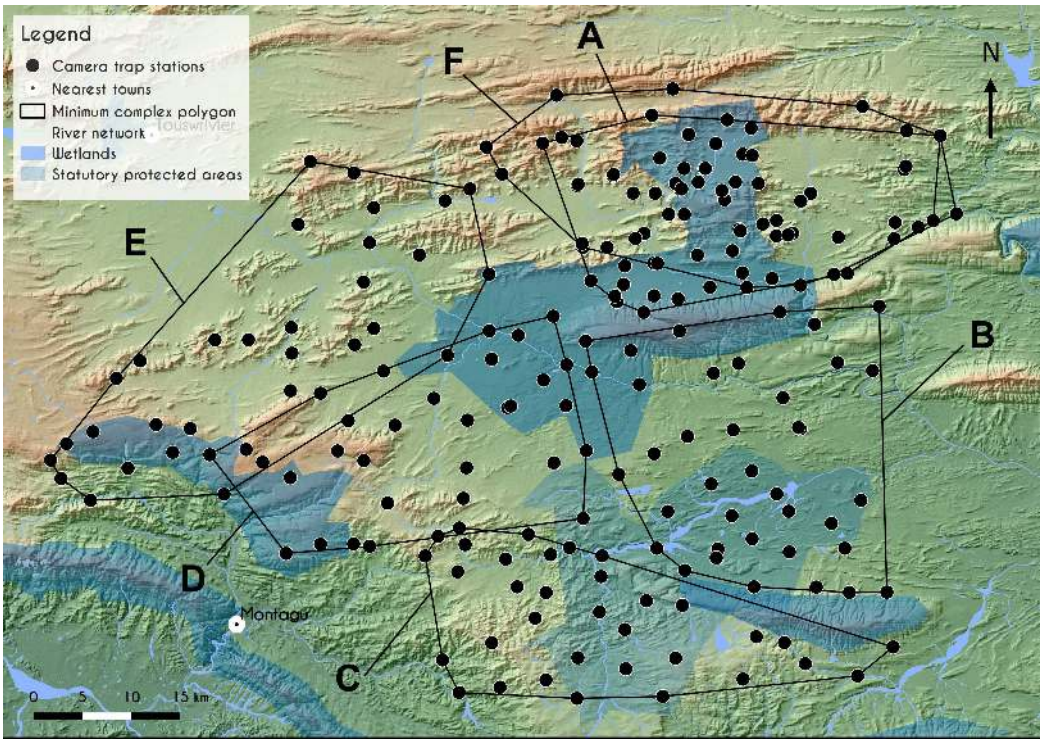

Figure 4.1: Sampling design.
Given the vastness of the study area (4,327 km^2) in the Little Karoo, the camera trap study was conducted as a series of six, three-month long, regional surveys (temporally and spatially separated): survey A, B, C, D, E and F. Every dot represents a camera trap station. Two months in survey A, the Little Karoo was hit by the worst flooding since 1981. The water level washed away 20 camera traps (a third), which were never to be found again. Survey A then led to redraw the scientific design and camera trap deployment protocol of the project. Camera trap stations were then all deployed on roads and animal paths, with a density of two camera trap stations per 50 km^2. Survey F consists of a replicate of survey A, using the newly chosen and standardised protocol which was then used throughout the project.

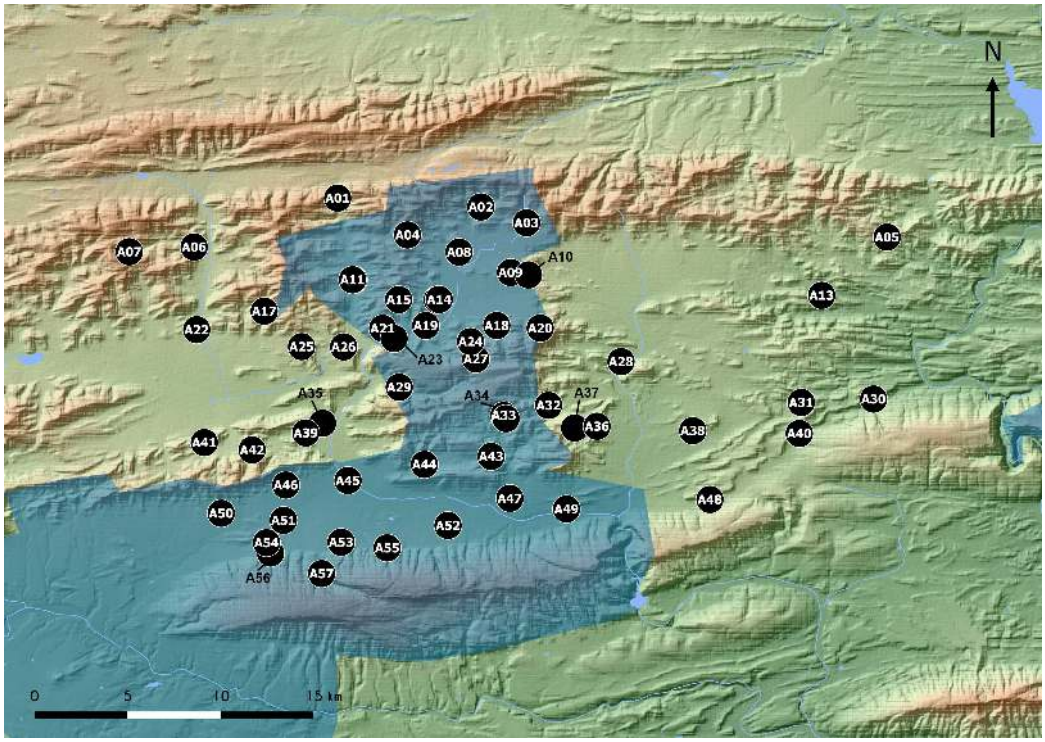

(a) Session A

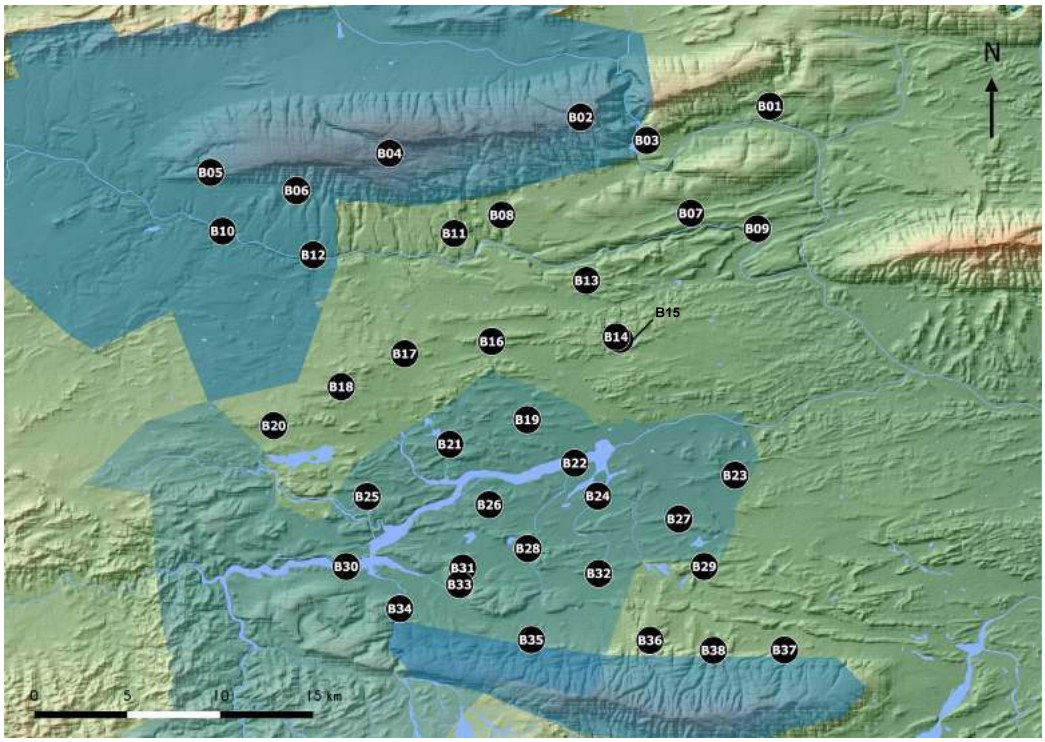

(b) Session B

Figure 4.1: Sampling design (continued).
A full caption is provided on p182.

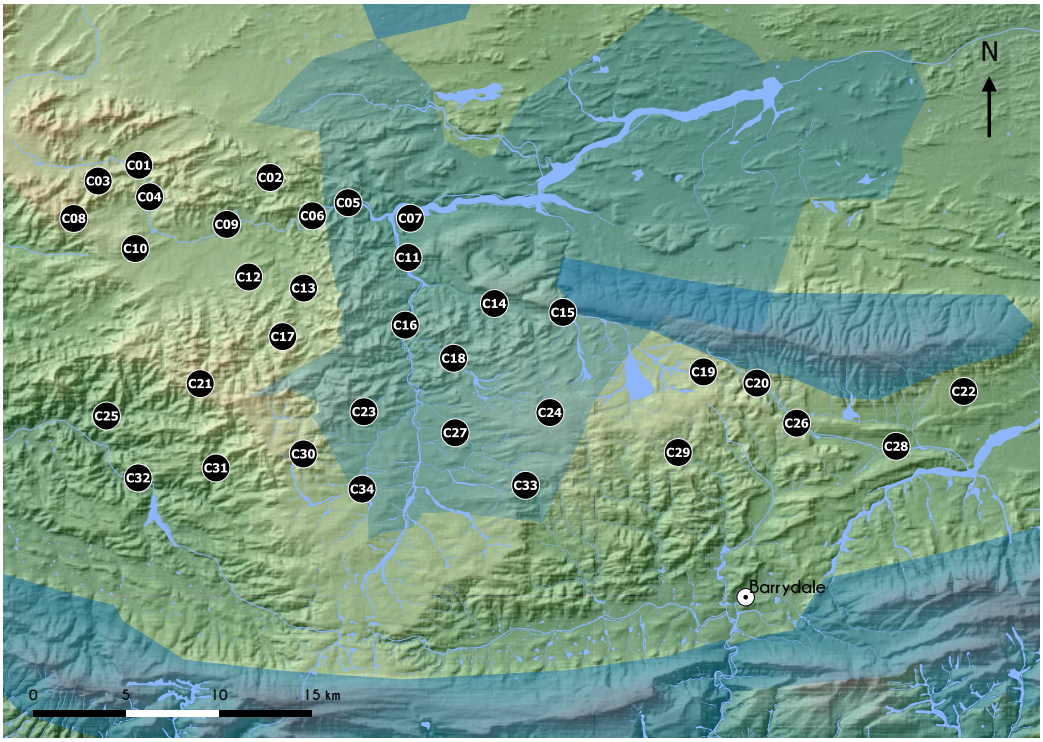

(c) Session C

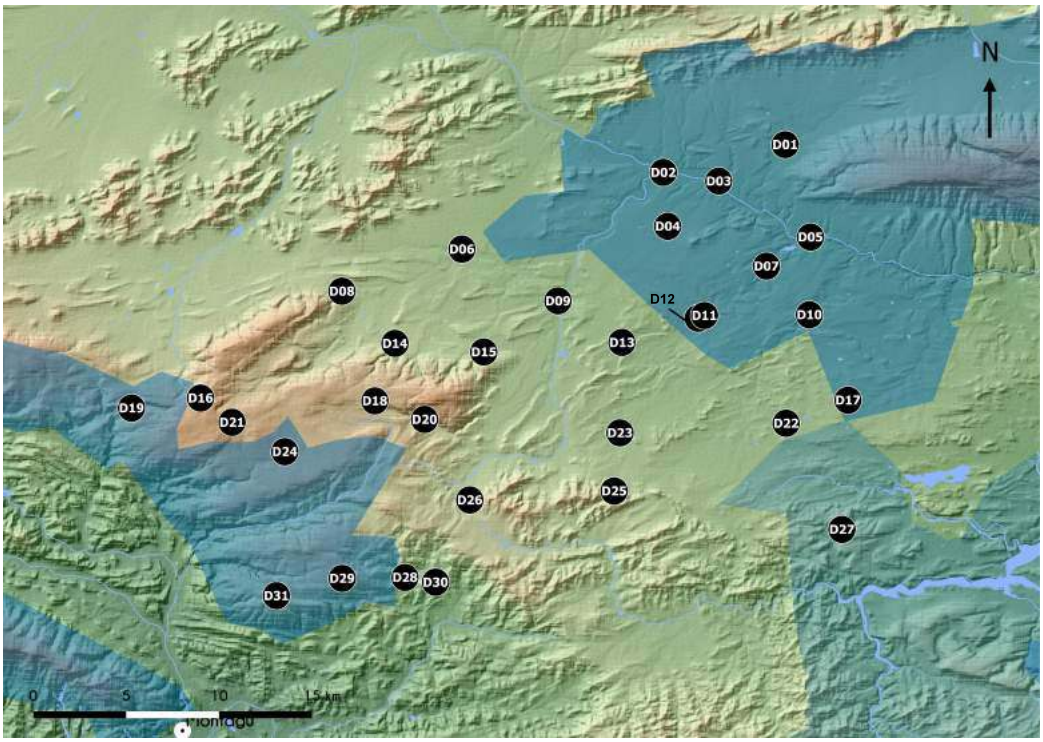

(d) Session D

Figure 4.1: Sampling design (continued).
A full caption is provided on p182.

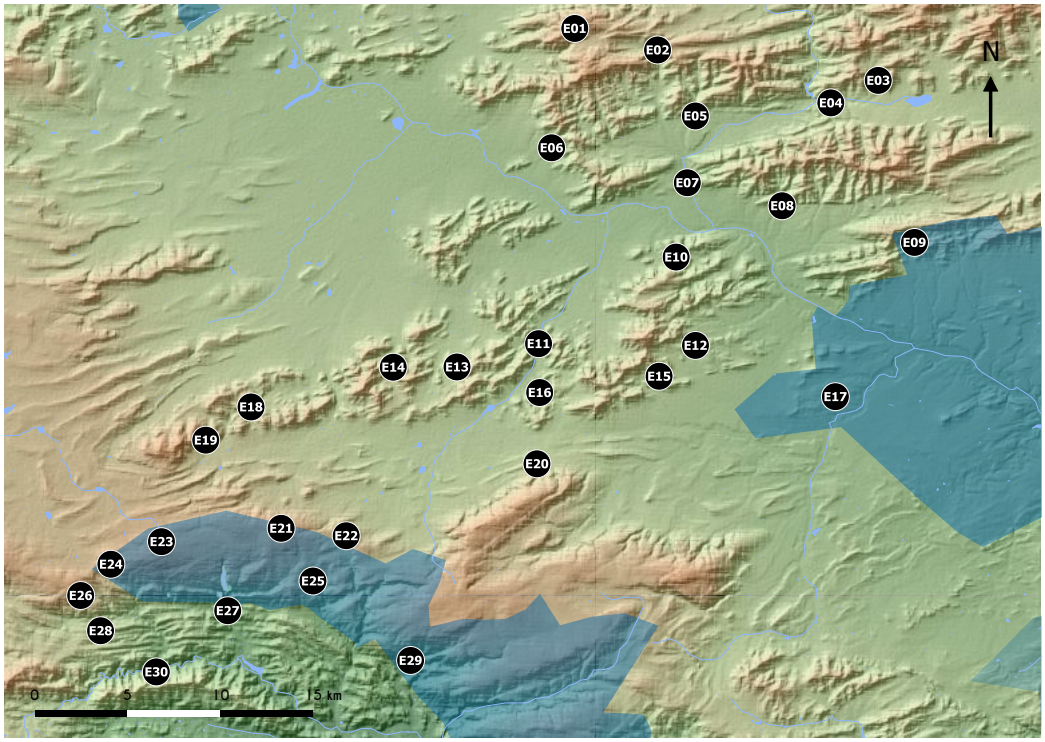

(e) Session E

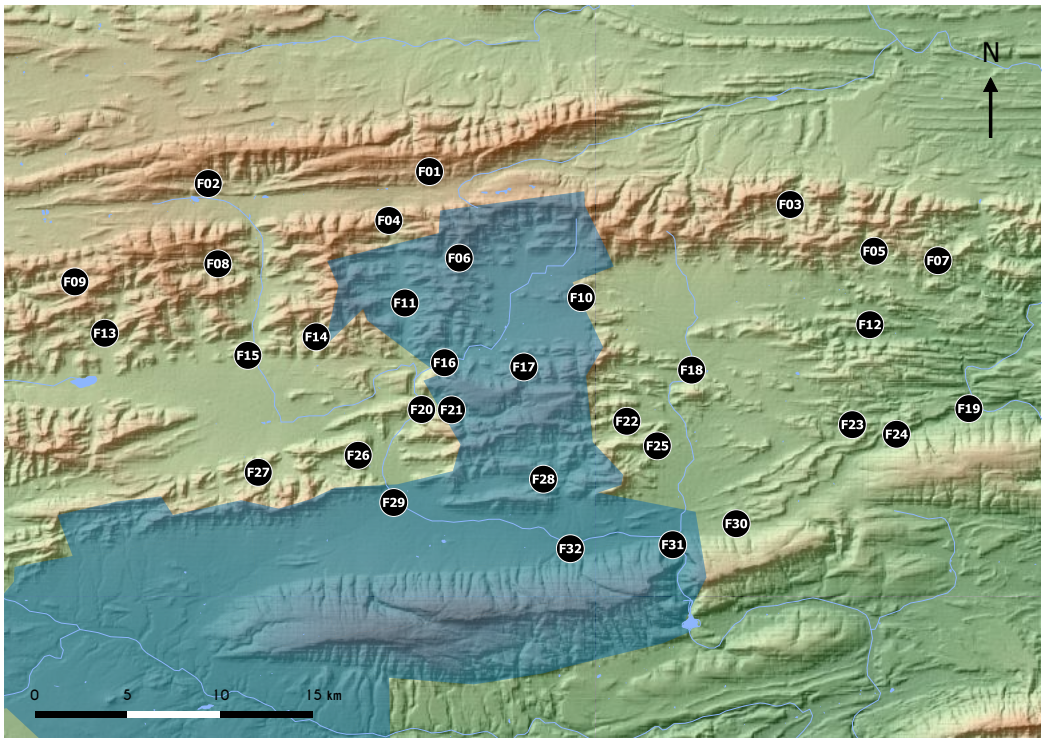

(f) Session F

Figure 4.1: Sampling design (continued).
A full caption is provided on p182.

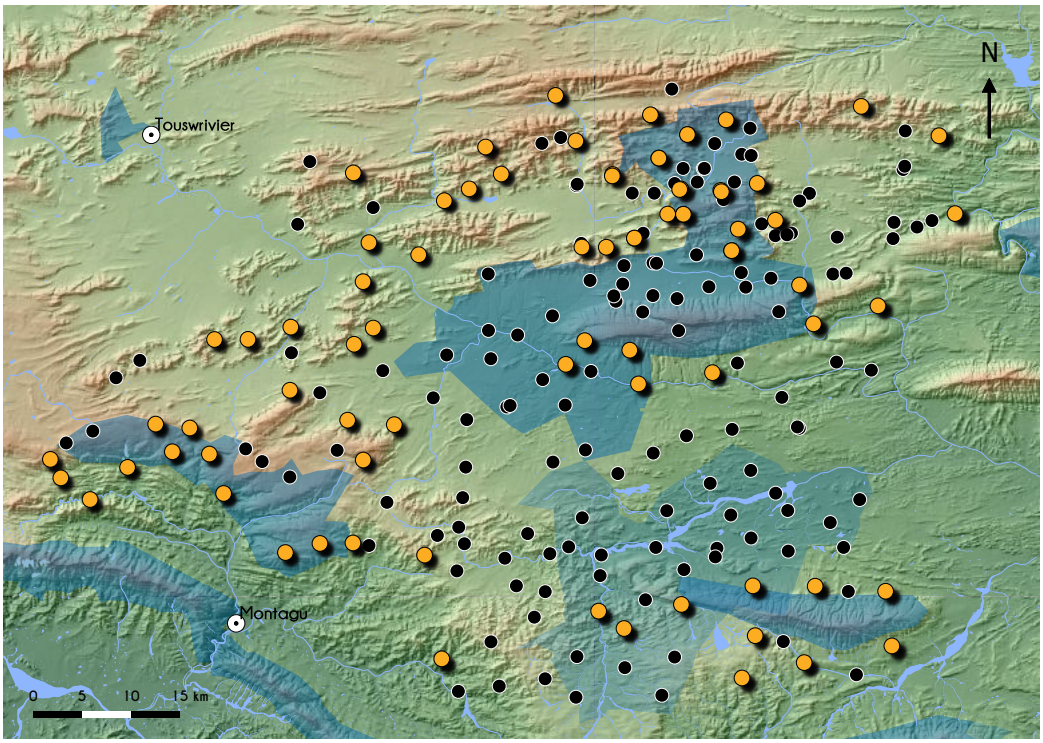

Figure 4.2: Photo-capture leopards.
The study provided 219 photo-captures of leopards in the Little Karoo, collected at 79 (35%) camera trap stations. Each point represents a camera trap station; the orange ones being those where leopards were photo-captured.

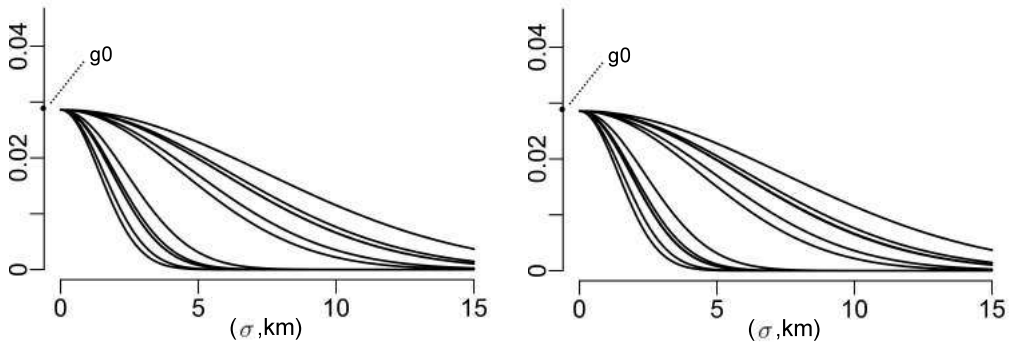

(a) Model 21 (b) Model 22

Figure 4.3: Detection functions.
The detection function is jointly defined by g0 (detection probability) and σ (index of home range size), and modelled as a halfnormal function. Each graph shows 12 curves (two classes $h2$, six sessions *session*); go (~ 1) being the sole intercept.

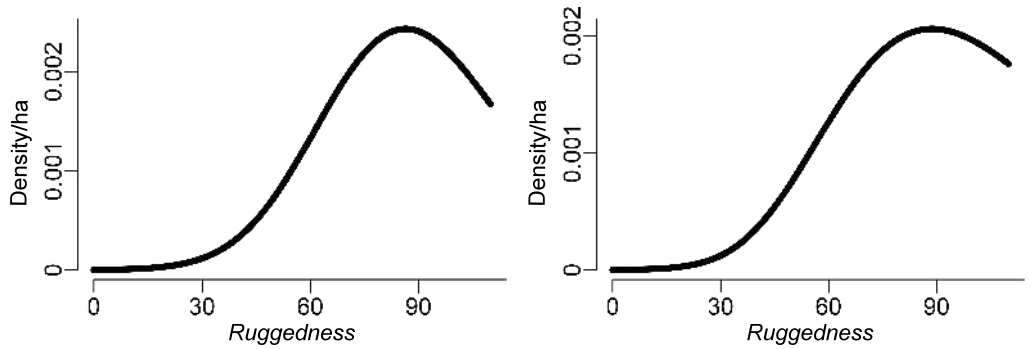

(a) Model 21 (b) Model 22

Figure 4.4: Density spline relationship with spatial covariate (ruggedness).
The curves show the relationship between the population density (second axis) and the terrain roughness (first axis).

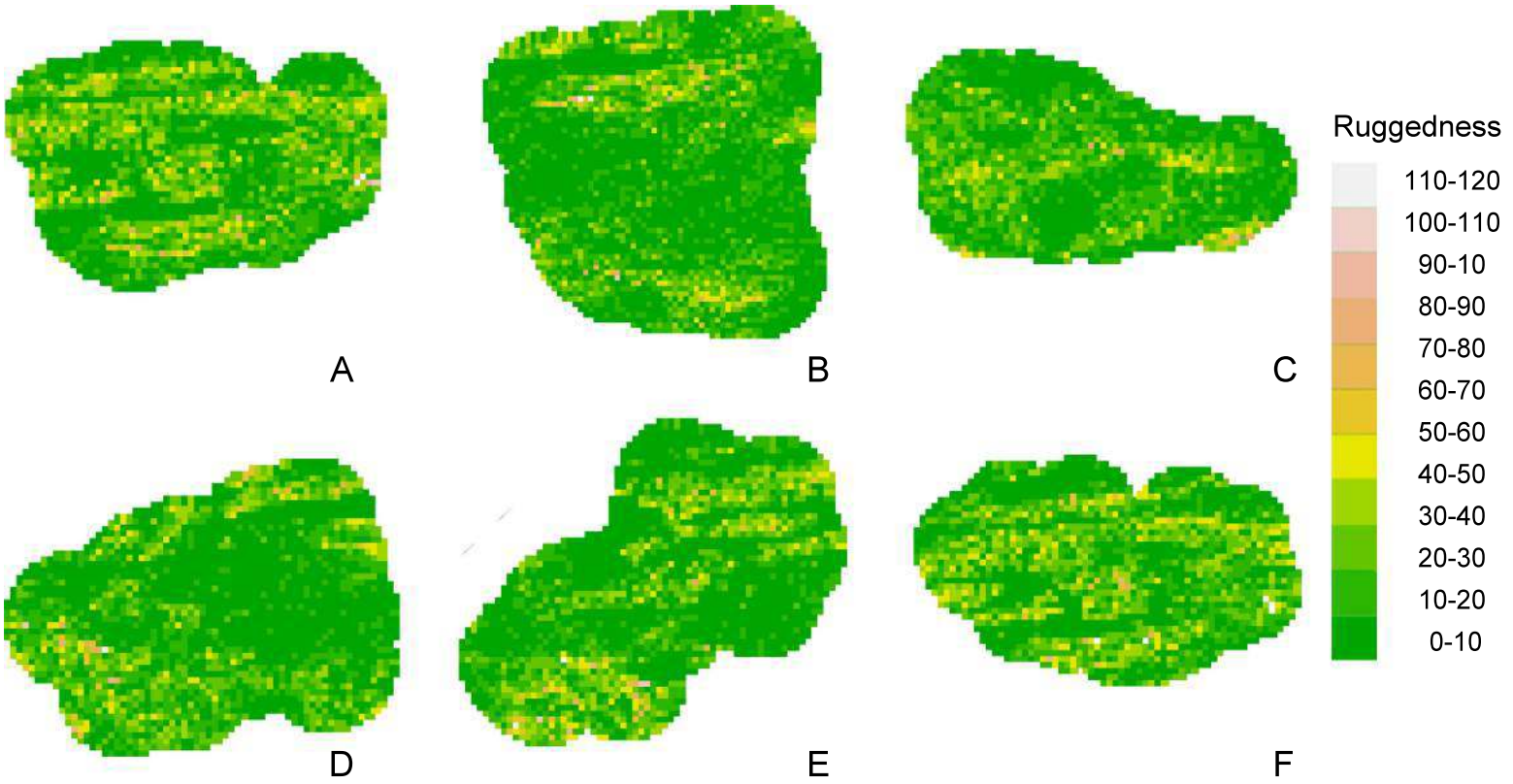

Figure 4.5: Ruggedness maps.
This figure shows the six habitat masks with ruggedness data (spatial covariate) that were constructed by the *secr.fit* function from the *secr* R-package version 3.1.0 [94], for the six regional surveys that took place in the Little Karoo.

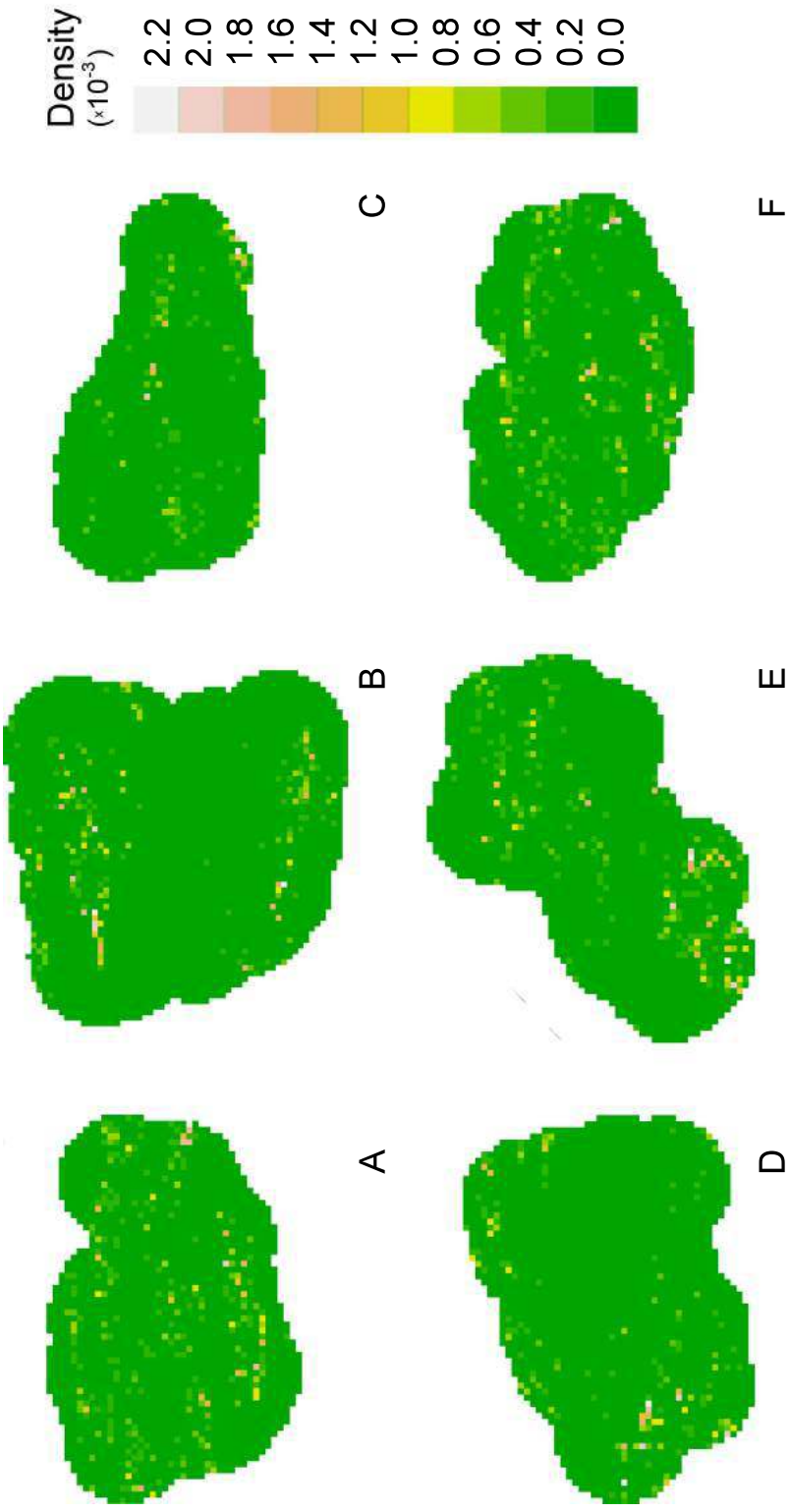

Figure 4.6: Density maps.
This figure shows the six predicted density maps from best-performing Model 22, for the six regional surveys that took place in the Little Karoo.